

Chapter 3

Continuity of high series opacity

3.1 Introduction

The present chapter focuses on calculating opacity consistently in a single spectral series from low lying discrete member lines through to the continuum within the escape factor framework. This is done by analytically extending the usual bound-bound definitions of the escape probabilities and absorption factors into bound-free regimes. It is shown that blended high series lines merge with a broadened continuum smoothly across the series limit with no need to introduce an ionising microfield which effectively ‘dissolves’ high quantum shells into the continuum. The continuous escape probabilities are evaluated in a new code and used to adjust high series and bound-free continuum emergent intensities for opacity. Similarly the continuous absorption factors are used to modify high series spontaneous emission and free electron recombination rates for population calculation in an analogous manner to their bound-bound counterparts. This chapter considers only hydrogenic opacity, with the recognition that the theory can be extended to non-hydrogenic elements.

3.2 Analytic continuity

Expressions (1.8) and (1.14) are the starting points for demonstrating analytic continuity. In the following algebra, bound-bound quantities are denoted either by the

subscripts ‘nn’ or ‘bb’, and the bound-free quantities with subscripts ‘bf’ or ‘ $n\kappa$ ’ with no change in meaning. We seek to show that

$$\Lambda_{bb}(\underline{r}) = 1 - \frac{\int \alpha_{bb}(\nu, \underline{r}) I(\nu, \underline{r}) d\nu}{\int \int_{\Omega} \varepsilon_{bb}(\nu, \underline{r}) d\Omega d\nu} \quad (3.1)$$

continues analytically into

$$\Lambda_{bf}(r) = 1 - \frac{\int \alpha_{bf}(\nu, \underline{r}) I(\nu, \underline{r}) d\nu}{\int \int_{\Omega} \varepsilon_{bf}(\nu, \underline{r}) d\Omega d\nu} \quad (3.2)$$

and that

$$\Theta_{bb} = \frac{\int_{\Delta\nu} \int_0^b \varepsilon_{bb}(\nu, l) e^{-\int_l^b \alpha_{bb}(\nu, l') dl'} dl d\nu}{\int_{\Delta\nu} \int_0^b \varepsilon_{bb}(\nu, l) dl d\nu} \quad (3.3)$$

continues into

$$\Theta_{bf} = \frac{\int_{\Delta\nu} \int_0^b \varepsilon_{bf}(\nu, l) e^{-\int_l^b \alpha_{bf}(\nu, l') dl'} dl d\nu}{\int_{\Delta\nu} \int_0^b \varepsilon_{bf}(\nu, l) dl d\nu} \quad (3.4)$$

The b-b and b-f emission and absorption coefficients are defined in chapter 1. We seek to prove, upon transformation of $n' \rightarrow i\kappa$, that $\varepsilon_{bb} \rightarrow \varepsilon_{bf}$ and $\alpha_{bb} \rightarrow \alpha_{bf}$, leading to continuity in Θ and Λ . For clarity, the ε and α expressions are reproduced below.

$$\varepsilon_{bb}(\nu) = \frac{1}{4\pi} N_{n'} A_{n' \rightarrow n} \phi_{n'n}(\nu) \quad (3.5)$$

will continue into

$$\begin{aligned} \varepsilon_{bf}(\nu) d\nu &= \frac{1}{4\pi} [N_i f(v) b_{\kappa} dv] [N_e v \sigma_{\kappa n}] \\ \Rightarrow \varepsilon_{bf}(\nu) &= \frac{1}{4\pi} [N_i f(v) b_{\kappa} dv] \left[N_e v \sigma_{\kappa n} \frac{1}{d\kappa} \right] \frac{d\kappa}{d\nu} \end{aligned} \quad (3.6)$$

with $f(v)$ being the Maxwellian velocity distribution for free electrons and $\sigma_{\kappa n}$ is the target area for free electron capture, given by

$$\sigma_{\kappa n} = \frac{2^4}{3\sqrt{3}} \frac{e^2 \hbar}{m^2 c^3} \frac{1}{\left[\frac{1}{n^2} + \frac{1}{\kappa^2}\right]} \frac{\kappa^2}{n^3} g_{\kappa n}^{II} \quad (3.7)$$

Similarly

$$\alpha_{nn'}(\nu) = N_n \frac{\pi e^2}{mc} f'_{nn'} \phi_{nn'}(\nu) g_{nn'}^I \quad (3.8)$$

will continue into

$$\alpha_{n\kappa}(\nu) = N_n \frac{\pi e^2}{mc} f'_{n\kappa} \frac{d\kappa}{d\nu} g_{n\kappa}^{II} \quad (3.9)$$

Note that the proofs shown here hold for NLTE population distributions with the inclusion of b-factors, b_n , for bound states which continue into b_κ factors for free states (representing deviations from a Maxwellian free-electron velocity distribution).

3.2.1 Continuity of emission coefficient

The resultant emission rate to level n for a given series, once the profiles start to blend together at high series members, is simply the sum of the b-b emission rates over all transitions in the series. That is,

$$\varepsilon_n(\nu) = \frac{1}{4\pi} \sum_{n'} N_{n'} A_{n' \rightarrow n} \phi_{n'n}(\nu) \quad (3.10)$$

As the series limit is approached, only nearby profiles contribute, the values of $N_{n'}$ and $A_{n' \rightarrow n}$ do not vary significantly and can be replaced by representative values $N_{\bar{n}'}$ and $A_{\bar{n}' \rightarrow n}$ and taken out of the summation. The emission rate to level n then becomes

$$\varepsilon_n(\nu) = \frac{1}{4\pi} N_{\bar{n}'} A_{\bar{n}' \rightarrow n} \sum_{n'} \phi_{n'n}(\nu) \quad (3.11)$$

For high series members, the profiles broaden and tend to the same basic distribution, only shifted slightly in frequency due to the increased energy of the upper level. We calculate the average emission rate over a small frequency interval, equal to the separation between line centres $\Delta\nu$

$$\varepsilon_n(\nu) = \frac{1}{4\pi} N_{\bar{n}'} A_{\bar{n}' \rightarrow n} \frac{1}{\Delta\nu} \int_{\Delta\nu} \sum_{n'} \phi_{n'n}(\nu) d\nu \quad (3.12)$$

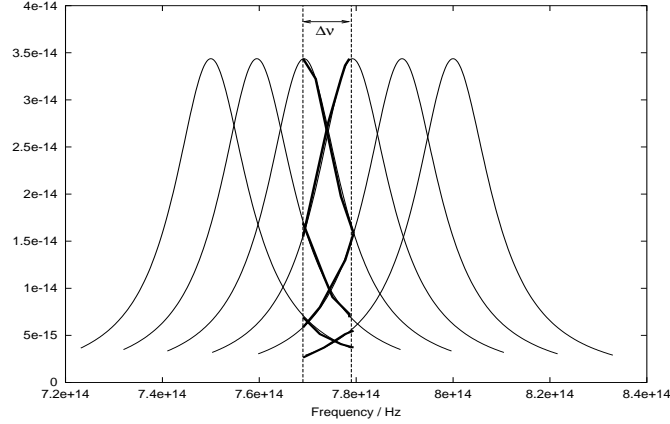


Figure 3.1: Diagram illustrating the contribution of overlapping profiles to the integration in eqn (3.12). Consider the contribution from each profile to the region of integration within the dotted lines. If one traces out the contributions from each profile in turn (see the bold segments of the profiles) it is equivalent to integrating over one normalised profile.

For high series members $\phi_{n'n}(\nu)$ is approximately the same for adjacent profiles, only shifted in frequency by $\Delta\nu$. As can be seen from figure 3.1, the summation inside the integral simply serves to select adjacent segments from the normalised profiles, and in the case of figure 3.1 we have an integral over one complete profile. If the region $\Delta\nu$ is then increased to cover $\Delta\bar{n}'$ profiles, the integral would be over $\Delta\bar{n}'$ normalised profiles. Thus the integral over $\Delta\nu$ reduces to $\Delta\bar{n}'$ (i.e. the number of line centres within the $\Delta\nu$ frequency region). Note that as our frequency element approaches the series limit, broadened profiles from the continuum form part of this contribution to the $\Delta\nu$ region (this is most clearly seen in the numerical simulation later in this section). In the limit of $\Delta\nu$ becoming very small, the average over the frequency region tends to $d\bar{n}'/d\nu$. Thus the number of spontaneous emissions over the region $d\nu$ is given by

$$\varepsilon_n(\nu) = \frac{1}{4\pi} N_{\bar{n}'} A_{\bar{n}' \rightarrow n} \frac{d\bar{n}'}{d\nu} \quad (3.13)$$

This is then analytically extended to continuum states using expressions for $N_{\bar{n}'}$ and $A_{\bar{n}' \rightarrow n}$ transformed into the continuum. That is,

$$N_{\bar{n}'} = N_e N_i \left[\frac{h^2}{2\pi m k T_e} \right]^{\frac{3}{2}} \frac{\omega_{\bar{n}'}}{2} \exp \left[\frac{I_{\bar{n}'}}{k T_e} \right] b_{\bar{n}'} \quad (3.14)$$

is extended into free states by letting $\bar{n}' \rightarrow i\kappa$ and using

$$\omega_\kappa = \frac{8\pi m^3 v^2 dv}{N_e h^3} \quad (3.15)$$

for the statistical weight of an electron in state κ (Menzel & Pekeris, 1935). The continuum statistical weight is defined over a momentum and volume element and is defined such that it is consistent with ω_n , that is there is no ω_+ term for the statistical weight of the ion. Also use

$$I_{\bar{n}'} = \frac{R z_0^2}{n'^2} \quad (3.16)$$

for the ionisation potential of level \bar{n}' . Thus

$$\begin{aligned} N_{\bar{n}'n} &\rightarrow N_e N_i \left[\frac{h^2}{2\pi m k T_e} \right]^{\frac{3}{2}} \frac{1}{2} \frac{8\pi m^3 v^2 dv}{N_e h^3} \exp \left[-\frac{R z_0^2}{\kappa^2 k T_e} \right] b_\kappa \\ &= N_i 4\pi v^2 \left[\frac{1}{2\pi k T_e} \right]^{\frac{3}{2}} \exp \left[-\frac{R z_0^2}{\kappa^2 k T_e} \right] b_\kappa \frac{m^3}{m^{\frac{3}{2}}} dv \\ &= N_i 4\pi v^2 \left[\frac{m}{2\pi k T_e} \right]^{\frac{3}{2}} \exp \left[-\frac{R z_0^2}{\kappa^2 k T_e} \right] b_\kappa dv \end{aligned} \quad (3.17)$$

The Maxwellian velocity distribution, $f(v)$ is given by

$$f(v) dv = 4\pi v^2 \left[\frac{m}{2\pi k T_e} \right]^{\frac{3}{2}} \exp \left[-\frac{m v^2}{2 k T_e} \right] dv \quad (3.18)$$

and the energy (E_κ) of the free electron is

$$E_\kappa = \frac{1}{2} m v^2 = \frac{R z_0^2}{\kappa^2} \quad (3.19)$$

Thus letting $n' \rightarrow i\kappa$ in equation (3.17) gives

$$N_{n'n} \rightarrow N_i f(v) b_\kappa dv \quad (3.20)$$

To transform the A-values, express A in terms of oscillator strengths, i.e.

$$A_{\bar{n}' \rightarrow n} = \frac{\omega_n}{\omega_{\bar{n}'}} \frac{8\pi^2 e^2}{mc^3} \nu_{\bar{n}'n}^2 f'_{\bar{n}'n} g_{\bar{n}'n}^I \quad (3.21)$$

and use

$$\nu_{\bar{n}'n} = \frac{Rz_0^2}{h} \left[\frac{1}{n^2} - \frac{1}{\bar{n}'^2} \right] \quad (3.22)$$

and

$$f'_{\bar{n}'n} = \frac{2^6}{3\sqrt{3}\pi} \frac{1}{\omega_n} \frac{1}{\left[\frac{1}{n^2} - \frac{1}{\bar{n}'^2} \right]^3} \frac{1}{n^3 \bar{n}'^3} \quad (3.23)$$

to obtain

$$\begin{aligned} A_{\bar{n}' \rightarrow n} &= \frac{\omega_n}{\omega_{\bar{n}'}} \frac{8\pi^2 e^2}{mc^3} \left(\frac{Rz_0^2}{h} \right)^2 \left[\frac{1}{n^2} - \frac{1}{\bar{n}'^2} \right]^2 \frac{2^6}{3\sqrt{3}\pi} \frac{1}{\omega_n} \frac{1}{\left[\frac{1}{n^2} - \frac{1}{\bar{n}'^2} \right]^3} \frac{1}{n^3 \bar{n}'^3} g_{\bar{n}'n}^I \\ &= \frac{1}{\omega_{\bar{n}'}} \frac{8\pi^2 e^2}{mc^3} \left(\frac{Rz_0^2}{h} \right)^2 \frac{2^6}{3\sqrt{3}\pi} \frac{1}{\left[\frac{1}{n^2} - \frac{1}{\bar{n}'^2} \right]} \frac{1}{n^3 \bar{n}'^3} g_{\bar{n}'n}^I \end{aligned} \quad (3.24)$$

Letting $n \rightarrow i\kappa$ and using eqn (3.15) for the statistical weight of an electron in the continuum gives

$$\begin{aligned} A_{\bar{n}' \rightarrow n} &\rightarrow -\frac{N_e h^3}{8\pi m^3 v^2 dv} \frac{8\pi^2 e^2}{mc^3} \frac{R^2 z_0^4}{h^2} \frac{2^6}{3\sqrt{3}\pi} \frac{1}{\left[\frac{1}{n^2} + \frac{1}{\kappa^2} \right]} \frac{1}{n^3 \kappa^3} g_{\kappa n}^{II} \\ &= \frac{N_e h}{v^2 dv} \frac{e^2}{m^4 c^3} R^2 z_0^4 \frac{2^6}{3\sqrt{3}} \frac{1}{\left[\frac{1}{n^2} + \frac{1}{\kappa^2} \right]} \frac{1}{n^3 \kappa^3} g_{\kappa n}^{II} \end{aligned} \quad (3.25)$$

Then using

$$\frac{1}{2} m v^2 = \frac{Rz_0^2}{\kappa^2} \quad (3.26)$$

to convert the dv into $d\kappa$ via

$$dv = -\frac{1}{mv} \frac{2Rz_0^2}{\kappa^3} d\kappa \quad (3.27)$$

The transformed A-value is

$$\begin{aligned} A_{\bar{n}' \rightarrow n} &\rightarrow \left[-N_e h \frac{1}{v^2} \frac{1}{dv} \frac{e^2}{m^4 c^3} R^2 z_0^4 \right] \left[\frac{2^6}{3\sqrt{3}} \frac{1}{\left[\frac{1}{n^2} + \frac{1}{\kappa^2}\right]} \frac{1}{n^3 \kappa^3} g_{\kappa n}^{II} \right] \\ &= -N_e h \left[\frac{m\kappa^2}{2Rz_0^2} \right] \left[-\frac{mv\kappa^3}{2Rz_0^2 d\kappa} \right] \frac{e^2}{m^4 c^3} R^2 z_0^4 \left[\frac{2^6}{3\sqrt{3}} \frac{1}{\left[\frac{1}{n^2} + \frac{1}{\kappa^2}\right]} \frac{1}{n^3 \kappa^3} g_{\kappa n}^{II} \right] \\ &= \left[N_e v \frac{2^4}{3\sqrt{3}} \frac{e^2 h}{m^2 c^3} \frac{1}{\left[\frac{1}{n^2} + \frac{1}{\kappa^2}\right]} \frac{\kappa^2}{n^3} g_{\kappa n}^{II} \frac{1}{d\kappa} \right] \\ &= N_e v \sigma_{\kappa n} \frac{1}{d\kappa} \end{aligned} \quad (3.28)$$

which is the bound-free emission rate.

Thus the bound-bound emission coefficient continues smoothly into the bound-free expression as $\bar{n}' \rightarrow i\kappa$. That is

$$\varepsilon_{\bar{n}' \rightarrow n}(\nu) \longrightarrow \frac{1}{4\pi} [N_i f(v) dv] \left[N_e v \sigma_{\kappa n} \frac{1}{d\kappa} \right] \frac{d\kappa}{d\nu} \quad (3.29)$$

and analytic continuity between equations (3.5) and (3.6) has been shown. A code was written to demonstrate the continuity of the resultant emission coefficient across the series limit. Both Lorentzian profile expressions and the expression of Griem (1960) could be used in the calculation, and existing ADAS subroutines were used to evaluate the necessary Gaunt factors, A-values and population b-factors. For the demonstration shown here, Lorentzian profiles are used throughout. Note that the proof outlined here works independently of the choice of line profile, the only necessity has been that the line profiles must be normalised. In practice one would use appropriate line profile expressions and widths for the plasma under investigation. See chapter 5 for an opacity calculation using the profile expression of Griem.

The code takes the same approach in treating the continuity as the proof shown above. That is, a wavelength element is considered in the spectrum and the contributions

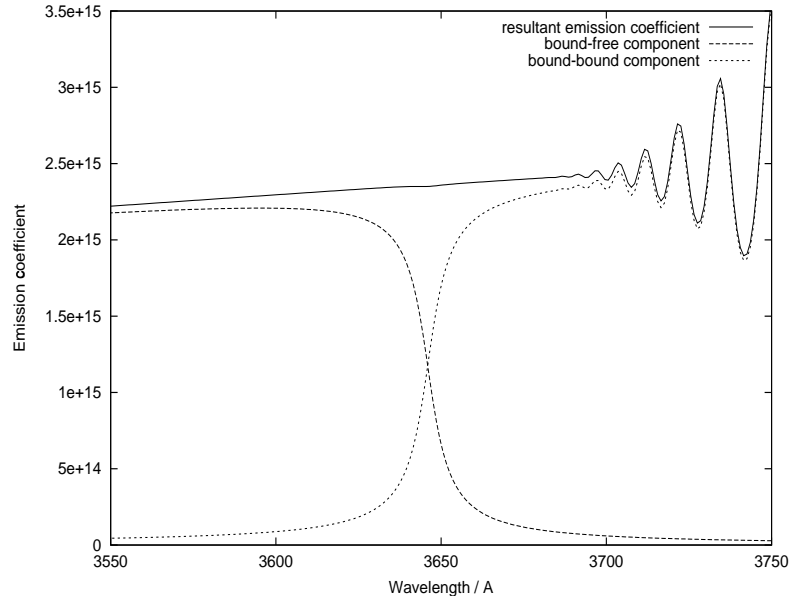


Figure 3.2: Emission coefficient for the Balmer series plotted across the series limit. The code was run for $N_e = 2 \times 10^{14} \text{ cm}^{-3}$, $T_e = 1 \text{ eV}$. Note that the continuum contribution is made up of a continuous set of bound-free line profiles.

from all line and continuum profiles to this element are evaluated. This region is then scanned across the series limit and the results plotted. In the blended region and continuum this wavelength segment corresponds to an ‘element’ of population, made up from the continuous free states or the pseudo-continuous highly excited states. At low series wavelengths the main contribution to the wavelength element is from the sum of all bound-bound profiles. As one approaches the series limit, and the states become indistinguishable and it is more appropriate to model this summation as an integral of the contributing profiles over energy. The continuum is modelled as a continuous set of line profiles (assumed Lorentzian with constant width), and the contribution to the wavelength element found from the integral over energy of these bound-free profiles. The resultant emission coefficient in the wavelength element is the sum of the bound-bound and bound-free contributions. The results are shown in figure 3.2.

Note that the bound-bound profiles make a contribution at continuum wavelengths and similarly the broadened continuum contributes at bound-bound wavelengths. It is

the combination of these contributions which leads to the smooth continuation across the series limit of the emission coefficient. b-factors were calculated for all transitions, though for the higher transitions they are equal to one. A maxwellian velocity distribution was assumed (i.e. $b_\kappa = 1$). However, the proof of continuity is for emission from an element of population in the continuum, which is then ‘scanned’ down into bound states. Thus the expected emission resulting from a non-Maxwellian distribution of free electrons can be modelled with the introduction of the appropriate b_κ values. Note that the emission coefficient well into the continuum is made up from all the contributing bound-free profiles and is equal to the usual analytic expression used to model the continuum profile (equation (3.6)). The approach of continuity shown here is significantly different from the conventional approach, whereby an ionising microfield is introduced. See section 3.3 for a discussion on this point.

3.2.2 Continuity of absorption coefficient

In a similar manner the bound-bound absorption coefficient, equation (3.8), continues into its corresponding bound-free expression, equation (3.9). Starting with the bound-bound absorption coefficient expression, for absorption to high n-shells the upper levels become progressively closer together until adjacent absorption profiles start to overlap. The number of absorptions at frequency ν due to all the overlapping lines is

$$\alpha_n(\nu) = N_n \frac{\pi e^2}{mc} \sum_{n'} f'_{nn'} g_{nn'}^I \phi_{nn'}(\nu) \quad (3.30)$$

The average of this quantity over a small frequency region $\Delta\nu$ is

$$\alpha_n(\nu) = N_n \frac{\pi e^2}{mc} \frac{1}{\Delta\nu} \int_{\Delta\nu} \sum_{n'} f'_{nn'} g_{nn'}^I \phi_{nn'}(\nu) d\nu \quad (3.31)$$

On approaching the series limit the profiles, $\phi_{nn'}$, that contribute to the $\Delta\nu$ region have approximately the same shape and are simply shifted along in frequency. The oscillator strength and Gaunt factor values for the contributing transitions can be replaced by representative values ($= f'_{n\bar{n}}$ and $g_{n\bar{n}}^I$). This produces

$$\alpha_n = N_n \frac{\pi e^2}{m c} f'_{n\bar{n}'} g_{n\bar{n}'}^I \frac{1}{\Delta\nu} \int_{\Delta\nu} \sum_{n'} \phi_{nn'}(\nu) d\nu \quad (3.32)$$

Again considering $\Delta\nu$ equal to the separation between the line profiles a similar argument to the emission case holds. The effect of the summation is to contribute adjacent components in the line profile to the integral such that the integration is effectively over the number of line centres in $\Delta\nu$. Because the profiles are normalised, the integral reduces to $\Delta\bar{n}'$ and as $\Delta\nu$ becomes infinitesimally small the integral tends to $d\bar{n}'$. The absorption coefficient then becomes

$$\alpha_{n\bar{n}'}(\nu) = N_n \frac{\pi e^2}{m c} f'_{n\bar{n}'} g_{n\bar{n}'}^I \frac{d\bar{n}'}{d\nu} \quad (3.33)$$

$g_{n\bar{n}'}^I \rightarrow g_{n\kappa}^{II}$ as shown in Burgess & Summers (1987) and $f'_{n\bar{n}'} \rightarrow -f'_{n\kappa}$ as seen in the definitions from Menzel & Pekeris (1935). From equation (3.22)

$$\frac{d\bar{n}'}{d\nu} \rightarrow -\frac{d\kappa}{d\nu} \quad (3.34)$$

It is now clear that equation (3.33) continues into equation (3.9) on transforming $n' \rightarrow i\kappa$. That is,

$$\begin{aligned} \alpha_{n\bar{n}'}(\nu) &\rightarrow N_n \frac{\pi e^2}{m c} g_{n\kappa}^{II} (-f'_{n\kappa}) \left(-\frac{d\kappa}{d\nu} \right) \\ &= N_n \frac{\pi e^2}{m c} g_{n\kappa}^{II} f'_{n\kappa} \frac{d\kappa}{d\nu} \\ &= \alpha_{n\kappa}(\nu) \end{aligned} \quad (3.35)$$

The continuous absorption coefficient was also evaluated numerically. Using the same technique as for the emission coefficient, the contributions to a wavelength element were evaluated and this wavelength element ‘scanned’ across the series limit. The continuum contribution is modelled as the integral over free energies of the contributing continuum profiles (assumed Lorentzian in the calculation shown here). The bound-bound contribution is evaluated from the sum of all series profiles at low series wavelengths, and as an integral over bound energies after a certain wavelength cutoff. In practice it was found that the sum over all bound-bound profiles could be extended

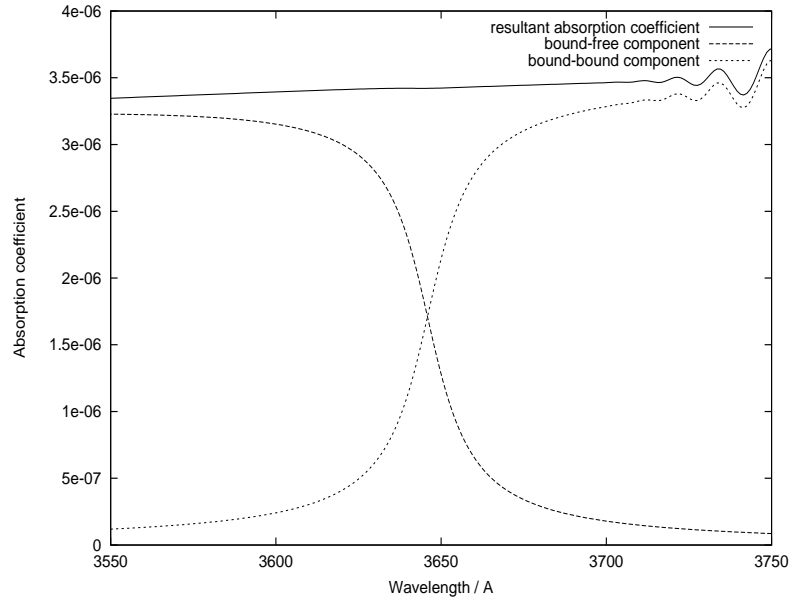


Figure 3.3: Absorption coefficient for the Balmer series plotted across the series limit. The code was run for $N_e = 2 \times 10^{14} \text{ cm}^{-3}$, $T_e = 1 \text{ eV}$.

to sufficiently high profiles to catch all the details of the integration. The results are shown in figure 3.3.

Thus analytic continuity in each quantity in the absorption factor and escape probability equations has been shown and the bound-bound absorption factors and escape probabilities continue smoothly into the corresponding bound-free expressions. This has been evaluated for two practical examples in section 3.4.

3.3 Contrast with the occupation probability formalism

There is an alternative approach to deal with the detailed treatment of the line blending near the series limit. The work stems from the original analysis of Inglis & Teller (1939) who derived an equation relating the last observable series line to the local electron density. As a rough estimate the continuum is often considered to advance down to this ‘spurious continuum edge’. A more detailed treatment is to introduce

a plasma microfield (set up by the fluctuating ions in the vicinity of the emitting atom or ion) to achieve smooth merging of blended lines into the continuum. The argument is that this field introduces a potential which can ionise highly excited electrons, thus there exists a quantum level above which electrons will be ionised before they have the chance to spontaneously decay to a lower level and electrons in these excited states will behave as if they were effectively free electrons. An ‘occupation probability’ can be evaluated, giving the probability that an excited electron is effectively ‘dissolved’ into the continuum. This approach has been widely used both in modelling series emission profiles and in collisional-radiative calculations. It was introduced by Gurovich & Engel’sht (1977) to obtain a non-divergent partition function and by Pigarov et al. (1998) in his modelling of atomic populations and emergent fluxes for Balmer series limit calculations.

Hubney et al. (1994) introduce an occupation probability, developed in Hummer & Mihalas (1988), in their stellar atmospheres code to include the effects of line blending near the series limit. It is instructive to examine their expression for the total absorption coefficient, derived from equation (2.4) of Hubney et al. (1994):

$$\alpha_n = N_n \left[\sum_{n' > n} \omega_{n'} \frac{\pi e^2}{mc} f_{n'n} \Phi_{n'n}(\nu) + \begin{cases} \sum_{n' > n} (1 - \omega_{n'}) \frac{\pi e^2}{mc} \frac{df_{n'n}}{d\nu} & \nu < \nu_{nn'} \\ \sigma_{n\kappa} & \nu > \nu_{nn'} \end{cases} \right] \quad (3.36)$$

where $\sigma_{n\kappa}$ is equivalent to our bound-free absorption coefficient. The similarities with equations (3.30) and (3.33) are evident. The main difference is the introduction of the factor ω_n which they refer to as the ‘dissolution factor’. Their blended line contribution is gradually reduced by this factor while the continuation of the bound-free absorption coefficient to bound-bound wavelengths is simultaneously increased. Thus as one approaches the series limit the absorption coefficient is driven to the extended continuum value by the microfield. Note that the continuum is treated as a profile with a sharp edge, not as a sum of bound-free profiles.

This approach differs from ours in that we have shown that the blended profiles along with the broadened continuum contribution give emission and absorption coefficients which merge smoothly through to the continuum, without any need to introduce an ionising microfield. The technique of modifying the statistical balance equations with

a level dissolution factor is incorrect on the grounds of detailed balance and energy conservation. Of course the microfield effects must be included in the collisional-radiative equations and the line broadening expressions to allow the populations and profiles to be accurately evaluated. The microfield effects on the line profiles are already included in this work with the use of the PPP broadening code. The inclusion of the microfield within the collisional-radiative framework as a rate with a corresponding inverse process is left for future work. The idea is that the microfield's effect on the populations are primarily due to individual ions moving closer than the nearest neighbour distance. These ions can remove an electron possibly via a charge exchange mechanism. This allows incorporation of the microfield as a process satisfying microreversibility consistently within the collisional-radiative framework and is planned for the next stage of ADAS development. Thus although the final continuous coefficients in this chapter are similar to those produced by the occupation probability method, the philosophies of the two approaches are quite different.

To the author's knowledge the generic proof of continuity shown here which holds for any physical set of line profiles has not been demonstrated before, with most authors opting for the occupation probability method. The closest example of the proof of this chapter is found in Seaton (1990). He considers the case of no line dissolution (i.e. no microfield effects) and states that the sum of many overlapping high series line profiles (considered to be step functions) in the high series absorption coefficient tends towards the photo-ionisation rate. However he then goes on to use an occupation probability approach to deal with series limits in his modelling of atomic data for hydrogen for the Iron project.

3.4 The use of continuous escape and absorption expressions

The absorption factor and escape probability expressions can now be evaluated. Such quantities can already be evaluated for discrete spectral lines (see chapter 2) and for continuum radiation (Drawin, 1970). Using the continuity theory shown here,

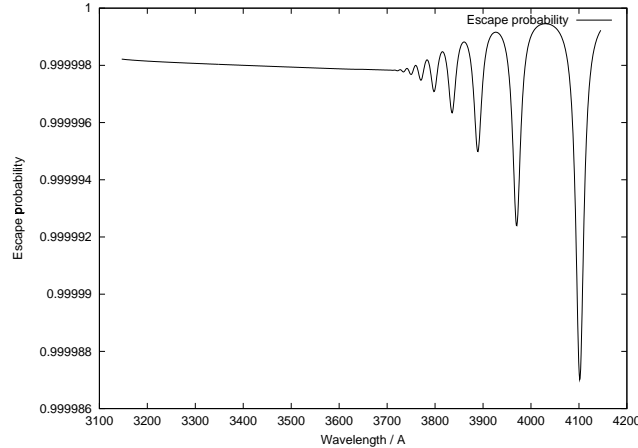


Figure 3.4: Continuous escape probability plotted for the case of the Balmer series in the fusion divertor. $N_e = 1 \times 10^{14} \text{ cm}^{-3}$, $T_e = 1 \text{ eV}$, length=5cm, assuming Lorentzian profiles and a Maxwellian velocity distribution for the free electrons. Note the smooth merging of the escape probability across the series limit.

this can be extended to include elements ‘within’ the blended high series region and continuum. The continuous emission and absorption coefficients are combined to produce the necessary opacity expression as a function of plasma parameters.

3.4.1 Some illustrations

Escape probability evaluated

Using the resultant ε and α expressions it is possible to evaluate Θ across the series limit. Consider a homogeneous plasma such that ε and α are independent of position. Equation (3.3) reduces to

$$\Theta = \frac{\int_{\Delta\nu} \frac{\varepsilon(\nu)}{\alpha(\nu)} (1 - e^{-\alpha(\nu)b}) d\nu}{b \int_{\Delta\nu} \varepsilon(\nu) d\nu} \quad (3.37)$$

Consider the Balmer series limit in fusion divertor plasmas. This region is expected to be optically thin, with the lower Lyman members being the only thick lines. Nevertheless it provides a useful check on our method. The escape probability code was run for $N_e = 1 \times 10^{14} \text{ cm}^{-3}$, $T_e = 1 \text{ eV}$, $b = 5 \text{ cm}$, the results are shown in figure 3.4.

It can be seen that the escape factor for the Balmer lines through to and including

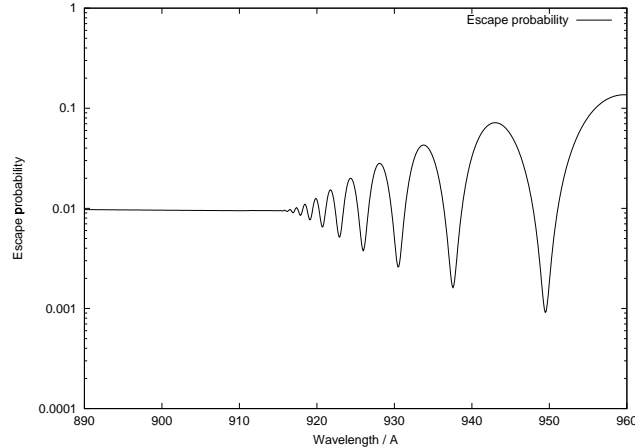


Figure 3.5: Continuous escape probability plotted for the case of the Lyman series in solar prominences. $N_e = 1 \times 10^{10} \text{cm}^{-3}$, $T_e = 1 \text{eV}$, $\text{length} = 1 \times 10^8 \text{cm}$. Only electron broadened Lorentzian profiles were used in this calculation. The Lyman series limit occurs at $\sim 911 \text{ \AA}$.

the continuum is, for all practical purposes, optically thin. Note that Θ continues smoothly across the series limit ($\sim 3645 \text{ \AA}$).

Next consider the case of the Lyman series limit in solar prominences. In this case one expects the Lyman lines and continuum to be extremely optically thick. It should be noted that the atomic populations in a solar prominence are strongly controlled by photo-absorption of incident radiation and that a full radiative transfer approach is required to accurately model the populations, fluxes and exact line profile shapes (see Gouttebroze et al., 1993). We use the solar prominence case as a check to see if the continuum expressions developed here can predict reasonable continuum opacities which smoothly merge into high series opacities. Thus Θ was evaluated for $N_e = 1 \times 10^{10} \text{cm}^{-3}$, $T_e = 1 \text{eV}$, $b = 1 \times 10^8 \text{cm}$, the results are shown in figure 3.5. Note that there is indeed significant opacity at continuum wavelengths and a smooth merging of Θ into bound-bound opacity across the series limit ($\sim 911 \text{ \AA}$).

Absorption factors evaluated

The generic expression for an absorption factor in terms of the continuous absorption and emission coefficients is

$$\Lambda = 1 - \frac{\int_{\Delta\nu} \alpha_n(\nu, \underline{r}) I(\nu, \underline{r}) d\nu}{\int_{\Omega} \int_{\Delta\nu} \varepsilon_n(\nu, \underline{r}) d\nu d\Omega} \quad (3.38)$$

In the evaluation of Λ , the intensity term is evaluated by integrating the emission, attenuated by photo-absorption, over the volume of the plasma to get the resultant intensity at the point of interest. For the case of Λ at the centre of a homogeneous density plasma of spherical geometry (of radius b) the absorption factor reduces to

$$\Lambda = \frac{\int_{\Delta\nu} \varepsilon(\nu) e^{-b\alpha(\nu)} d\nu}{\int_{\Delta\nu} \varepsilon(\nu) d\nu} \quad (3.39)$$

Figure 3.6 shows the results for the Lyman series limit at expected solar prominence conditions. Λ is evaluated as a function of frequency to produce the absorption factor across the series limit. However, for adjustments to atomic population or free electron distributions it is necessary to define a population element (and hence a frequency element) for which to calculate the Λ factors.

Defining $\Delta\nu$ accordingly gives the expression most appropriate to our desired application. With $\Delta\nu$ covering one complete spectral line it is possible to generate the usual discrete line absorption factors. With $\Delta\nu$ chosen to be a small element, the absorption factor corresponding to a small population element below the continuum edge, or in the continuum itself can be found. If $\Delta\nu$ is chosen to cover $\kappa = \infty \rightarrow 0$ (i.e. $\nu = \nu_i \rightarrow \infty$, with ν_i the frequency at the continuum edge), we average over the whole continuum and get the same expression as Drawin (1970), i.e.

$$\begin{aligned} \Lambda_i &= 1 + \frac{1}{n_z n_e R_i} \left[\frac{\pi e^2}{m_o c} n_{z-1,i} \int_{\nu_i}^{\infty} u(\nu, \underline{r}) \frac{df}{d\nu} d\nu \right] \\ &= 1 - \frac{1}{n_z n_e R_i} \left[\frac{\pi e^2}{m_o c} n_{z-1,i} \int_{\nu_i}^{\infty} u(\nu, \underline{r}) f'_{n\kappa} g_{n\kappa}^{II} \frac{h\kappa^3}{2Rz_0^2} d\nu \right] \end{aligned}$$

where $(n_z n_e R_i)$ is the recombination rate from the continuum to level i

However, if $\Delta\nu$ is chosen to be smaller than this we can examine recombination from different parts of the Maxwellian distribution of free electrons. This could then be used to look at the population distribution ‘inside’ the continuum and thus to investigate photo-ionisation driven non-Maxwellian free electron distributions.

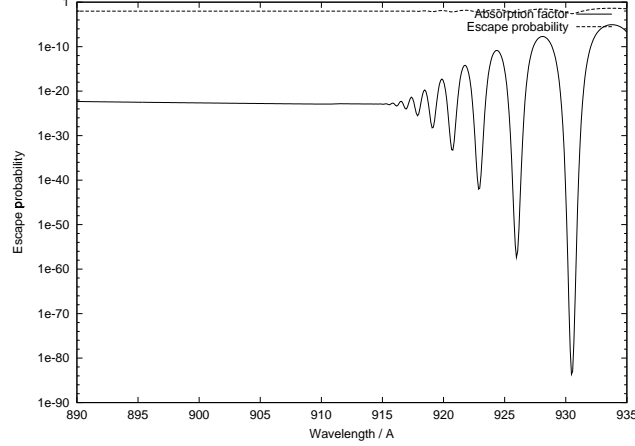


Figure 3.6: Absorption factor plotted for the Lyman series limit for typical prominence parameters. The code was run for $N_e = 1 \times 10^{10} \text{ cm}^{-3}$, length = $1 \times 10^8 \text{ cm}$, $T_e = 1 \text{ eV}$

Note that for the situation shown, the absorption factor is significantly less than the escape factor at the same wavelength. This indicates the case where a photon has a chance of escaping along a given line of sight, but the probability of a photo-absorption at the centre of the plasma is very large due to the large radiation field incident at the centre (generated by the rest of the plasma volume). In these circumstances there is a stronger influence on the optically thick populations than on the emergent flux. Note that we have replaced the notion of a high series level with a small frequency element corresponding to an element of population. We would then need to model all the possible rates to and from these elements. A means of incorporating a continuous Λ into the present collisional-radiative calculation would be to still consider photo-absorption and emission from a discrete level, but to evaluate the intensity term in equation (3.38) from the overlapping profiles. Thus we have the intensity at the point of interest as the resultant intensity due to all overlapping profiles, which can then be absorbed by an individual profile, or emitted from that same profile. That is, our absorption factor expression becomes.

$$\Lambda = 1 - \frac{\int_{\Delta\nu} \alpha_{discrete}(\nu) I_{blend}(\nu) d\nu}{\int_{\Omega} \int_{\Delta\nu} \varepsilon_{discrete}(\nu) d\nu d\Omega} \quad (3.40)$$

where the frequency integration is over the one high series spectral line profile, and the emission and absorption coefficients correspond to the values for that discrete

line, i.e. no line blending is accounted for. It is only in the intensity term that the fully blended emission and absorption coefficients are considered.

This approach has the advantage that it requires minimal changes to the existing collisional-radiative framework. Rates already exist for these high n-shells, and the Λ s evaluated here can be added directly, such a technique has been used in section 5.2.2.

One of the long term applications of this work is the investigation into non-Maxwellian free electron distributions. For this the specification of population ‘elements’ in the continuum and at high quantum shells would be necessary, and the more generic absorption factor expression is the appropriate one to use.

3.5 Conclusions

Analytic continuity of absorption factors and escape probabilities from bound through to free states has been shown. This allows opacity to be modelled in discrete spectral lines, blended high series lines and in the continuum. The approach shown here is contrasted with the occupation probability formalism and shown to be a more meaningful method of extending photo-rates across the ionisation threshold.

It should be noted that with the development of the analytically continuous emission coefficient in this chapter it is immediately possible to predict an emergent flux that continues smoothly from bound-bound to bound-free wavelengths for an optically thin plasma. This has been done for the case of the Balmer series limit in the fusion divertor and is described in section 5.3. The use of the escape probability and absorption factor expressions developed in this chapter allows this type of spectral feature generation to be extended to optically thick conditions (see section 5.2.2).